A new closed-loop regulation method dedicated to piezoelectric resonators based isolated DC-DC converter

Emile Bigot, Ghislain Despesse, Valentin Breton, François Costa

A NEW CLOSED-LOOP REGULATION METHOD DEDICATED TO PIEZOELECTRIC RESONATORS BASED ISOLATED DC-DC CONVERTER

Emile Bigot[1], Ghislain Despesse[1], Valentin Breton[1], François Costa[2]*

[1] CEA-Leti, Minatec Campus, University of Grenoble Alpes, 17 Avenue des Martyrs, 38054, Grenoble, France
[2] University Paris-Saclay, ENS Paris-Saclay, CNRS, SATIE University Paris-Est Créteil, 94010, Créteil, France
**emile.bigot@cea.fr*

Keywords: isolated DC-DC converter, closed-loop control, piezoelectric resonators (PRs).

Abstract

Magnetic components are widely used in power electronics. Yet, their downscaling with frequency becomes moderate from 100 kHz, which limits the possibility of reducing the volume of the passive components in power converters. Therefore, a major breakthrough is under investigation to replace such components with piezoelectric resonators. Though, the conversion implies the use of more complex conversion cycles. In the literature, they include at least one synchronisation on the mechanical strain and closed-loops to regulate the zero voltage switching operations and the power flow. In this paper, a new technique involving a single closed-loop control without any mechanical synchronisation is presented. To achieve this, a novel eight-phase conversion cycle has been designed and applied to a Dual active Bridge Isolated Piezoelectric Resonators Converter (DB-IPRC). This novel cycle simplifies the control without compromising the converter's power level and efficiency. The following study first introduces an analytical model that models the converter's switching operations. Then, a new analytical function is presented to estimate the converter's operating frequency. Subsequently, exploiting the unique features of the new switching sequence, the single closed-loop control is experienced on a DB-IPRC. The paper concludes on unchanged efficiency and power level compared to the open loop fine-tuned configuration.

1. Introduction

Magnetic components are limited in energy storage capabilities at high frequency. They exhibit high losses and are cumbersome in contemporary power converters. Therefore, the replacement of these components is under investigation for power application in the range of 1W to 10kW and with an operating frequency higher than 100 kHz. One solution is to use piezoelectric resonators (PRs). By setting them electrically into a mechanical resonance, it is possible to store and restore energy through a conversion cycle.

To be efficient, piezoelectric materials should have a high quality factor and express a high coupling factor. So far, hard lead zirconate titanate (hard-PZT) and lithium niobate (LNO) are good candidates for power conversion [1], [2]. Due to the high permittivity of PZT, their operating frequency is limited to frequencies under 2MHz, contrary to LNO which becomes of interest at operating frequency higher than 3MHz [2]. Around a specific resonant mode, PRs are modelled using the Van-Dyke model [3]. As shown in Figure 1, this model consists of a mechanical branch $\{R_m, L_m, C_m\}$ and a parallel electrical capacitive branch C_p. When used in a power converter, the PR operates between its resonant an anti-resonant frequency, where it exhibits an inductive behaviour, as presented on the impedance measurement of Figure 2.

Previous works have initially focused on the search for dedicated topologies to realize step-down, step-up and even isolated structures[4], [5], [6], [7]. Contrary to conventional inductor-based converters, the need for balancing charges in the PR during a conversion cycle implies the use of at least six phases in the conversion cycle, as presented in Figure 3. In addition, due to the parallel capacitance of the resonator, zero voltage switching operations are mandatory on the PR voltage. Thus, through a period of conversion, the PR alternates between open phases and clamped phases.

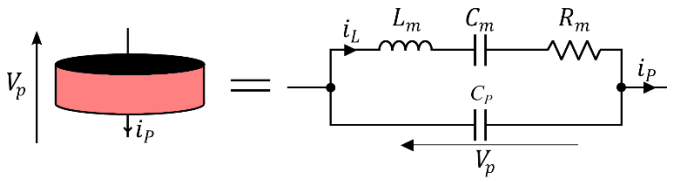

Figure 1: Piezoelectric Van-Dyke model around a specific resonant tone

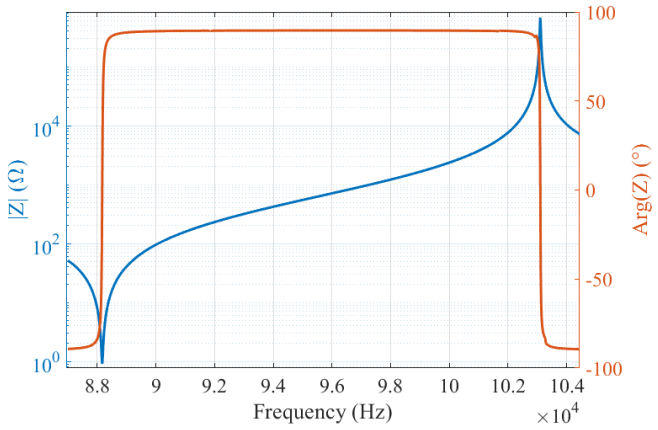

Figure 2: Bode diagram of a piezoelectric resonator between its resonant an anti-resonant frequency for a first radial resonant tone of a C213disk (25Dx2T) from Fujiceramic

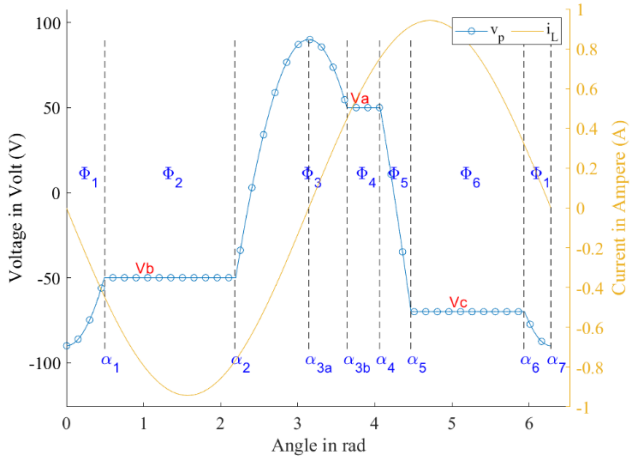

Figure 3: General six-phase conversion cycle for a PR Buck converter

This makes the control hard to achieve, requiring the calculation of multiple timings and the generation of multiple command signals.

Methods already exist to regulate the PR conversion cycle. Some synchronize the switching cycle with the PR inner current i_L, which is an image of the PR mechanical strain. This can be achieved through zero-crossing detection [8] of the current or by using a more complex, yet more robust PLL [9]. Achieving zero voltage switching involves measuring the voltage at the closing instant and regulating the charge exchange during the constant voltage phases. Finally, the output voltage regulation is done by adjusting the connection duration of the PR to the input, which corresponds to the energy-storing phase. However, implementing these commands is challenging due to the need for a convenient current synchronization and measurements of the resonator voltage v_p to achieve zero voltage switching. This implies the use of at least three imbricated closed-loops controls, one for the current/mechanical synchronization, one to achieve the required voltage swing, one to control the power flow. So far, this command has a limited frequency of operation around 100 kHz.

Another solution consists in applying a well-known conversion cycle a part of the time [10]. This method is similar to the conventional burst method, but it features persistent current circulation within the resonator. Unlike the previous method, the implementation is simplified and only needs the measurement of the output voltage. As a result, it scales well when used at high frequencies of operations. Nonetheless, the piezoelectric resonator is not operating at its optimum and low frequency voltage ripples are intrinsically present at the output.

This paper presents a new control method with a new smart eight-phase conversion cycle well suited to the dual active bridge isolated PR converter (DB-IPRC). In addition, we present a new analytical solution of the operating frequency for the converter operating set point $\{V_{in}, V_{out}, I_{out}\}$. Finally, by using the new simplified mathematical model and thanks to the self-balancing of the PRs internal energy, only one regulation loop based on the output voltage needs to be set. The loop measures the output voltage error and annihilate it by modifying the estimated output current. To compress the system, the loop embeds a rather accurate model of the converter that inputs the operating point $\{V_{in}, V_{out}, I_{out}\}$ and outputs the related switching angles and operating frequency. Also, using the eight-phase cycle in a step-down heightens the robustness of the control loop and allows some deviation against the mathematical model. In the end, neither synchronization with the PRs current, nor PRs voltage monitoring, which were previously challenging to achieve, are needed for the new regulation scheme.

In what follows, a first section presents the modeling of the new eight-phase conversion cycle and the determination of the operating frequency. Next, working on the DB-IPRC, we set up the regulation loop for the step-down operating mode and introduce the switching margins. Finally, the control scheme is implemented in a STM32G474RE that pilots the DB-IPRC. From this implementation multiple tests are conducted and the converter efficiency is measured.

2. Modeling of the regulation scheme

In this section, we briefly present the DB-IPRC structure and its constraints. Then we present the new eight-phase control

cycle and how it simplifies converter control without compromising its effectiveness. From this new cycle, a mathematical model is developed and a new frequency function is deduced. The section concludes with the introduction of the regulation scheme derived from the mathematical model.

2.1. *The DB-IPRC structure and its constraints*

This paper focuses on the control of the DB-IPRC structure shown in Figure 4. This structure allows insulating a primary side from a secondary side using the capacitive behaviour of two PRs. Since the two PRs are set in series, the total voltage cycle v_p is equal to:

$$v_p = v_{p1} + v_{p2} \tag{1}$$

Considering that PRs have quite the same impedance, the v_p voltage is considered well divided. Furthermore, each resonator operates around a V_{offset} voltage that is the low frequency common mode voltage between both sides of the converter:

$$v_{p1} = \frac{v_p}{2} + V_{offset} \tag{2.1}$$

$$v_{p2} = \frac{v_p}{2} - V_{offset} \tag{2.2}$$

To operate without introducing any high-frequency common mode voltage, the constant voltage phases have to be composed of combinations between input and output voltages. Therefore, only voltages in the series $\{V_{in}\text{-}V_{out},\ V_{out}\text{-}V_{in},\ V_{in}+V_{out},\ -V_{out}\text{-}V_{in}\}$ can be applied to the resonator overall potential v_p. In article [7] a six-phase cycle $\{V_a=V_{out}\text{-}V_{in},\ V_b=V_{in}\text{-}V_{out},\ V_c=-V_{out}\text{-}V_{in}\}$, as presented in Figure 3, was applied to the resonators. In order to reverse the polarity v_{pa} on the primary side, an extra voltage excursion to $\{V_{in}+V_{out}\}$ at angle α_{3a} has to be added. Since energy and charges must be balanced through a conversion cycle [7], the following constraints have to be respected:

$$Q_a + Q_b + Q_c = 0 \tag{2.1}$$

$$V_a Q_a + V_b Q_b + V_c Q_c = E_{PR_{loss}} \tag{2.2}$$

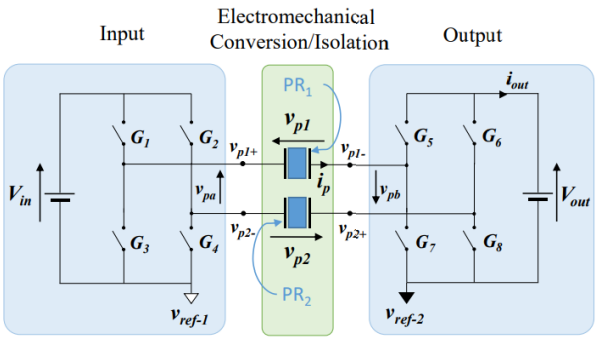

Figure 4: The DB-IPRC topology

With Q_k the exchanged charges during constant voltage phases and E_{PRloss} the energy losses in PRs during a cycle of conversion. Thanks to the high quality factor Q_m of the used resonators (>1000), the current i_L in the motional branch $\{R_m, C_m, L_m\}$ can be considered nearly sinusoidal as follows:

$$i_L(t) = -I_L \sin(\omega t) \tag{3}$$

An approximation of the amplitude I_L is done as in [2], with a separation into an "useful" part contributing to the output power and a "circulating" part which allows the self-voltage swing of the resonator. This leads to:

$$I_L = I_{useful} + I_{circulating} \tag{4}$$

In the case of the DB-IPRC topology and the conversion cycle used in [7], the total current is:

$$I_L = \frac{\pi}{2} I_{out} + \frac{C_p \omega (V_{in} + V_{out})}{2} \tag{5}$$

Finally, it appears that PRs are limited in term of inner current [2]. This means that the new eight-phase conversion cycle must not induces a higher current in the PRs for a specific operating point $\{V_{in}, V_{out}, I_{out}\}$ to not impact both efficiency and power capability of the converter. This constraint drives the construction design of the new eight-phase cycle.

2.2. *The eight-phase conversion cycle*

Insulation is an essential feature in the DB-IPRC, which prohibits the application of v_{pa}=0 and/or v_{pb}=0 as stated in [7]. This restriction limits the application to only four possible constant voltages on v_p. Using all feasible combinations, we establish the new step-down cycle as follows:

$$V_2 = -V_{in} + V_{out} \tag{6.1}$$

$$V_4 = V_{in} + V_{out} \tag{6.2}$$

$$V_6 = V_{in} - V_{out} \tag{6.3}$$

$$V_8 = -V_{in} - V_{out} \tag{6.4}$$

The key waveforms of the new eight-phase cycle are shown in Figure 5. Compared to the conventional six-phase cycle, the new eight-phase cycle is symmetrical, resulting in a reduced disparity due to the same conduction duration in distinct full-bridge. Moreover, since the PRs voltage amplitude remains the same, the circulating current amplitude remains the same. Similarly, the relation between I_{useful} and I_{out} remains unchanged. Thus, no change in the I_L current amplitude is observed when using the new eight-phase cycle, which allows equal conversion performance compared to the six-phase cycle. By using the symmetry only four distinct angles are necessary to control the cycle, and the following equations are imposed:

$$\alpha_{k+4} = \alpha_k + \pi \; with \; k \in [1:4] \quad (8)$$
$$Q_{k+4} = -Q_k \; with \; k \in \{1,2\} \quad (9)$$

Which leads the new eight-phase cycle to be balanced in terms of energy on each half period:

$$V_2 Q_2 + V_4 Q_4 = \frac{E_{PR_{Loss}}}{2} \quad (7.1)$$
$$V_6 Q_6 + V_8 Q_8 = \frac{E_{PR_{Loss}}}{2} \quad (7.2)$$

To construct the associated mathematical model, one can consider that when the resonator is in the clamped phase, the related resonance is due only to the mechanical branch {R_m, L_m, C_m}, while for the opened phase, the mechanical branch resonates {R_m, L_m, C_m} with the electrical branch C_p. The related pulsations are respectively the resonant and anti-resonant pulsations of the PR which are:

$$\omega_r = \frac{1}{\sqrt{L_s C_s}} \quad (10.1)$$
$$\omega_{ar} = \sqrt{\frac{(C_p + C_s)}{L_s C_s C_p}} \quad (10.2)$$

Due to high mechanical quality factor of the resonator, the current can be considered nearly sinusoidal during each conversion phase (i.e. opened and closed phases). Yet, at the switching instant α_k this current must respect continuity when

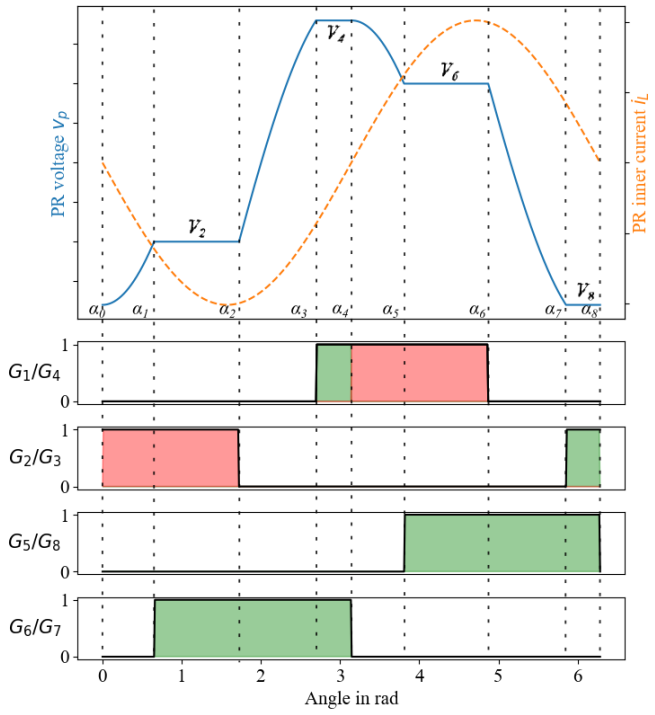

Figure 5:The 8-phase cycle with the related switches position Gi/j. Green areas correspond to natural diode conduction while red one corresponds to forced conduction and need a switch closing command applied to an active switch.

the resonator passes from a clamped phase to a free phase. This leads the current in the mechanical branch {R_m, L_m, C_m} to comply with the following relations:

$$\alpha_k = \omega_k t_k + \theta_k \quad (11.1)$$
$$i_{Lk}(t) = I_{Lk} \sin(\omega_k t + \theta_k) \quad (11.2)$$
$$I_{L(k+1)} = I_{Lk} \sqrt{1 - \left(\frac{\omega_k}{\omega_{k+1}}\right)^2 * \sin(\omega_k t_k + \theta_k)^2 + \left(\frac{\omega_k}{\omega_{k+1}}\right)^2} \quad (11.3)$$
$$\theta_{k+1} = arcos\left(\frac{I_{Lk}\omega_k}{I_{Lk+1}\omega_{k+1}} \cos(\omega_k t_k + \theta_k)\right) - \omega_{k+1} t_k \quad (11.4)$$

If the switching angles {α_1, α_2, α_3} are in the range of [*0.9 rad ;2.1 rad*], $I_{L(k+1)}$ can be considered approximately equal to I_{Lk} with an error in the evolution of I_{Lk} below 15%. This is the case when the conversion ratio is close to 0.5 and when the useful current I_{useful} is in the same order of magnitude than the circulating current I_{circul}. Therefore, the approximation works well for high voltage operating points (with a high ratio of circulating current, >0.3).

Next, integrating the current during the open phases and the clamped phases, the following relations are determined between each switching angles:

$$\alpha_0 = 0 \quad (12.1)$$
$$\alpha_1 = \mathrm{acos}\left(cos(\alpha_0) - (V_2 - V_8)/2C_p\omega_{ar}/I_L\right) \quad (12.2)$$
$$\alpha_2 = acos(cos(\alpha_1) + Q_2\omega_r/I_L) \quad (12.3)$$
$$\alpha_3 = \mathrm{acos}(cos(\alpha_2) - (V_4 - V_2)/2C_p\omega_{ar}/I_L) \quad (12.4)$$
$$\alpha_4 = acos(cos(\alpha_3) + Q_4\omega_r/I_L) \quad (12.5)$$

To determine the switching sequence, the last parameter to be determined is the operating frequency of the converter. Papers [11] and [12] present numerical solvers to obtain the operating frequency of specific topology and for a specific operating point {V_{in}, V_{out}, I_{out}}. Nonetheless, these computations are computationally intensive, making real-time estimation hard to achieve. In this paper, we assume that the current amplitude I_L remains constant while its related pulsation changes during the transition between successive phases. Therefore, we can construct an analytical function that determines the operating frequency based on the operating point as follows:

$$-2 = \frac{Q_2\omega_R}{I_L} + \frac{Q_4\omega_R}{I_L} + \frac{C_p\omega_{ar}}{I_L}\mathrm{V}_4 \quad (13)$$
$$\pi I_{out} + C_p\omega \mathrm{V}_4 = \frac{\pi I_{out}\omega_R}{\omega} + \frac{C_p\omega_{ar}}{I_L}\mathrm{V}_4 \quad (13.1)$$
$$\omega^2 C_p \Delta V + \omega\left(\pi I_{out} - C_p\omega_{ar}\mathrm{V}_4\right) - \pi I_{out}\omega_R = 0 \quad (13.2)$$
$$\Delta = \left(\pi I_{out} - C_p\omega_{ar}\mathrm{V}_4\right)^2 + 4C_p\mathrm{V}_4\pi I_{out}\omega_R \quad (13.3)$$
$$\omega = \frac{-\pi \mathrm{I}_{\mathrm{out}} + C_p\omega_{ar}\mathrm{V}_4 + \sqrt{\Delta}}{2C_p\mathrm{V}_4} \quad (13.4)$$

According to function (13.4), the estimation of the operating frequency for a specific operating point $\{V_{in}, V_{out} I_{out}\}$, is independent from PRs losses.

To conclude, in this part we have developed a mathematical model to approximate the switching angles and the operating frequency of the new eight-phase conversion cycle. Unlike the six-phase cycle, the eight-phase cycle naturally balances the energy in the PRs thanks to the symmetry imposed in the switching angles in equation (8). Therefore, it considerably reduces the number of angles to be determined.

2.3. The eight-phase cycle and its resilience against calculation errors

In the previous part, it has been observed that a theoretical model can be set in order to estimate the control variables of the converter, which are the frequency and the switching angles. This section aims to determine the sensitivity of the calculated variables and how a miscalculation can affect the converter's operation.

Starting with the operating frequency, we can state from Figure 2, that any error in the frequency estimation results in a shift in the equivalent impedance of the resonator. This, in turn, affects the desired output current for a given PR voltage swing. Therefore, for a given voltage swing, the i_p current amplitude deviates from the desired one leading to a change in the useful current I_{useful} in the resonator. In conclusion, an inaccurate frequency estimation can prevent the resonator from achieving the desired output current, as PRs operate at the wrong impedance.

Next, assuming that the switching angles are miscalculated, the converter's efficiency decreases. Indeed, for closing angles $\{\alpha_1; \alpha_3; \alpha_5; \alpha_7\}$, if the switching angles are under estimated, a hard-switching operation happened. This results in high switching losses due to the significant parallel capacitance of the PRs. However, delaying the switching angles $\{\alpha_1; \alpha_3; \alpha_5; \alpha_7\}$ results in the PRs voltages being clamped to the related constant voltage phases (i.e. V_2, V_4, V_6, V_8) thanks to the reverse diodes of the switches. This means that when the switching "on" command occurs, only losses due to the diode voltage drop happen. Nonetheless, at the beginning of the clamped phase, extra losses due to the conduction through the diode are present. Indeed, these losses do not increase with the operating frequency, which is not the case for the hard-switching losses. Therefore, delaying the calculated angles $\{\alpha_1; \alpha_3; \alpha_5; \alpha_7\}$ prevents any hard-switching operations during practical operations. Lastly the switching instants $\{\alpha_0; \alpha_4; \alpha_8\}$, are fixed and correspond to references in the conversion (i.e. 0, π, 2π). However, if there are errors in the mathematical model causing the charge equation balance (9) to be poorly respected, the transition of the internal current i_L in the PRs may not be well synchronized with the opening instants $\{\alpha_0; \alpha_4; \alpha_8\}$. This can result in the generation of additional reactive power in the PRs, particularly if the real instants are in advanced. To prevent this, secondary switches may be opened in advance. Thus, the reverse switches diodes always realize the end of the constant voltage phases V_4 and V_8, which permits to operate with the exact necessary amount of reactive power in the PRs. Finally, for the opening angles $\{\alpha_2; \alpha_6\}$, if the openings are advanced, switching angles $\{\alpha_3; \alpha_7\}$ are advanced, seemly for angles $\{\alpha_4; \alpha_8\}$ and finally angles $\{\alpha_1; \alpha_5\}$. Therefore, the energy furnish to the PRs during clamped phases $\{V_2; V_4\}$ remains the same but all the switching events occur earlier. Seamlessly, if the opening angles $\{\alpha_3; \alpha_7\}$ are delayed, all the other switching angles are delayed.

To conclude, the eight-phase cycle symmetry allows the natural synchronization of the applied voltage cycle on the PRs strain. Additionally, we have demonstrated that delaying the switching angles $\{\alpha_1; \alpha_3; \alpha_5; \alpha_7\}$ or advancing $\{\alpha_0; \alpha_4; \alpha_8\}$ does not significantly affect the converter's efficiency. This is mainly attributable to the possibility of conducting through the reverse switches diodes. Indeed, in the eight-phase cycle, the internal energy of PRs is adjusted through half a conversion cycle, and the conduction instants $\{\alpha_3; \alpha_7\}$ may start through the natural conduction diode of the associated switches. As shown in green in Figure 5 for G_1/G_4 and G_2/G_3 command signals, the margins are important and increase when the conversion ratio is diminished in order to maintain the energy balance over a half-period. In the end, compared to the calculated angles, the applied switching angles are changed as follow:

$$\alpha_{3+k} = \alpha_{3calc} + \alpha_{closeprim} \; with \; k \in \{0; 4\} \quad (14.1)$$

$$\alpha_{1+k} = \alpha_{1calc} + \alpha_{closesecond} \; with \; k \in \{0; 4\} \quad (14.2)$$

$$\alpha_{4+k} = \alpha_{4calc} - \alpha_{opensecond} \; with \; k \in \{0; 4\} \quad (14.3)$$

Where $\{\alpha_{closeprim}; \alpha_{closesecond}; \alpha_{closeopen}\}$ are fixed switching shifts added to the theoretical estimation to ensure soft operations without extra reactive energy in the PRs. Finally, to reach the desired operating point $\{V_{in}; V_{out}; I_{out}\}$, it is necessary to converge accurately on the operating frequency. This is the purpose of the following output voltage regulation loop.

2.4. The output voltage regulation loop

Based on the previous calculations, one can determine the switching angles and the operating frequency from the converter's operating point $\{V_{in}, V_{out}, I_{out}\}$.

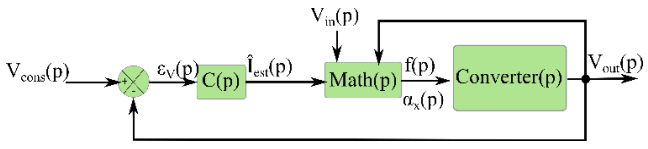

Figure 6: The output voltage regulation loop

Furthermore, angular shift can be applied within the allowed margins, to ensure efficient operation of the converter even with miscalculations of the switching angles. Yet, the frequency must be exact and in real operations, calculation errors occur. Indeed, the higher is the operating frequency, the higher is the piezoelectric impedance (see fig. 2), which results in a lower output current and thus in a lower output voltage. Consequently, to achieve accurate voltage, and so frequency regulation, we construct a single regulation loop.

As the impedance of the piezoelectric resonator is not linear, an intermediate parameter $\hat{I}_{est}$ is introduced; it represents an estimation of the output current and better fit with the output voltage variation. Furthermore, the introduction of this estimated extra parameter allows for the calculations of switching angles, as shown in equation (12). In the end, the regulation loop is constructed as follows. First the voltage error ε_V is used to generate an estimated current $\hat{I}_{est}$. Subsequently, the $\hat{I}_{est}$ parameter is translated into switching angles and operating frequency using the mathematical model and the inputs of the actual output voltage and input voltage. Nonetheless, the estimated current $\hat{I}_{est}$ may differ from the actual output current I_{out}. Still, the conduction margins described in the preceding section ensure efficient steady-state operation despite errors in angle calculations error. Therefore, cancelling the ε_V error enables to reach the genuine operating frequency on the PRs for the desired output voltage.

Finally, to compensate the voltage output error, an integral term is necessary in the corrector *C(p)*. For simplicity and robust operation, we opted to implement a *PI* corrector.

2.5. Conclusion of the theoretical modelling and control

In this first section, we analyse the PR behaviour and create a novel self-balanced energy cycle made of eight conversion phases. Afterwards, we note that most of the switching angles in this conversion cycle can be estimated with some errors. These errors are acceptable, as long as the switching takes place during the reverse diode conduction phase. Leveraging this information, we design a regulation loop that requires only two low frequency voltage measurements (V_{in} and V_{out}) to apply an efficient conversion cycle on the PRs.

3. Experimental measurements

The prototype is built using the DB-IPRC structure shown in Figure 4, with the components referenced in Table I. The experimental set-up is displayed in Figure 7. The disc resonators used are made of C213 materials from Fujiceramic and sized 25mm diameter by 1mm of thickness. Operating on the first radial resonant mode allows a clear impedance band of operation (as shown in Figure 2), free from any parasitic spurious mode. Also, the resonator requires operation in a frequency range of 89kHz to 103kHz.

To control the converter a Nucleo-G474RE development board which encompasses HR-TIMER has been chosen. These specific timers enable a high resolution with discrete step of 216ps that makes them ideal for high frequency driving. Moreover, since the developped regulation loop can be based on low-frequency observations, the refreshment of the regulation loop is set to 20kHz, cadenced by an internal timer. To ensure the insulation of the command on both the primary and the secondary side, numerical isolators IL711 are placed before gate drivers. Also, since the voltage measurements are not insulated, we consider a known voltage input which permits to remove input voltage measurment. By referencing the control board to the secondary part of the converter, it is possbile to directly evaluate the output voltage using the MCU's inner ADC.

Finally, to measure the efficiency of the converter, two HMC8015 power analyzers have been used.

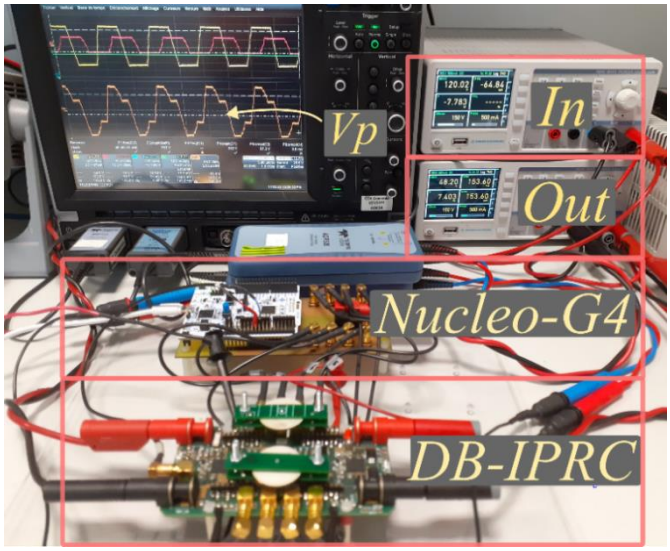

Figure 7: Experimental setup

TABLE I: Prototype netlist

Component	Reference
Piezoelectric resonators	25mm x 1mm, C213, *Fuji Ceramics*
Half bridges	600V, 10A, Mastergan1, *ST*
Parallel diodes	400V, 3A, ES3G-E3/57T, *Vishay*
Numerical isolator	IL711, *NVE Corporation*
Control board	Nucleo-G474RE, *ST*
Input capacitance	4.4µF, X7R
Output capacitance	4.4µF, X7R

3.1. *Implementation and test of the regulation loop*

The PI corrector is determined on the fastest operating point of the converter that occurs under light load operations. In our case, the corrector is sized to operate on a $1k\Omega$ light load. It results in the determination of an integration gain K_I of *1.0* and a proportional gain K_p of *5e-3*. As the implementation is digital, a sampling rate of 20*kHz* is set. Using the forward Euler method, the implementation results in:

$$\epsilon_V\big(T_e(k+1)\big) = V_{out}\big(\big(T_e(k+1)\big) - V_{out}(T_e k) \quad (15.1)$$

$$\hat{I}_{est}\big(T_e(k+1)\big) = \hat{I}_{est}(T_e k) + K_p\epsilon_V\big(T_e(k+1)\big) + K_I T_e \epsilon_V(T_e k) \quad (15.2)$$

To make the control robust, switching shifts $\{\alpha_{closeprim}; \alpha_{closesecond}; \alpha_{closeopen}\}$ are added to the calculation. In the implementation, we set them equal to 0.2 rad.

Various tests were performed to assess the converter's stability, as shown in Figure 8. It is observed from Figure 8.a that the output voltage response time at 95% is less than 2ms for light load operations. Subsequently, Figure 8.b demonstrates the new regulation's ability to converge on a new set point without any errors. In addition, it can be seen in this example that the response time changed due to the modification of the load. Which is in agreement with the theory, as the loading (R_{out}) in Figure 8.b is divided by 3 compared to the start event of Figure 8.a. This leads to a response time at 95% of 3 times greater than in Figure 8.a, i.e. 6ms. Finally, Figure 8.c illustrates the regulation's ability to apply an efficient conversion cycle on the resonator. First, no hard switching operations are observed on the resonator voltage, which means that no extra energy is lost during the closing of the converter switches. Secondly, we observe in Figure 8.c, that the evolution of v_p at instant $\{\alpha_0; \alpha_4\}$ begins with slopes close to zero, meaning a current i_L close to zero and then an opening of switches G_5 to G_8 on current zero crossing. It shows furthermore, that resonators embed just the amount of energy needed to achieve the voltage swing for soft switching operations.

To conclude, in this section, we describe the implementation of the PI controller in a stm32G474 microcontroller. Two examples of voltage set-point changes have been analyzed to see how the output voltage stabilizes. Next, in steady state, we show that soft switching operations are respected and that no extra reactive power is introduced. Finally, we propose to compare the converter efficiency with the one measured in [7] using the reference six-phase conversion cycle in open loop operation.

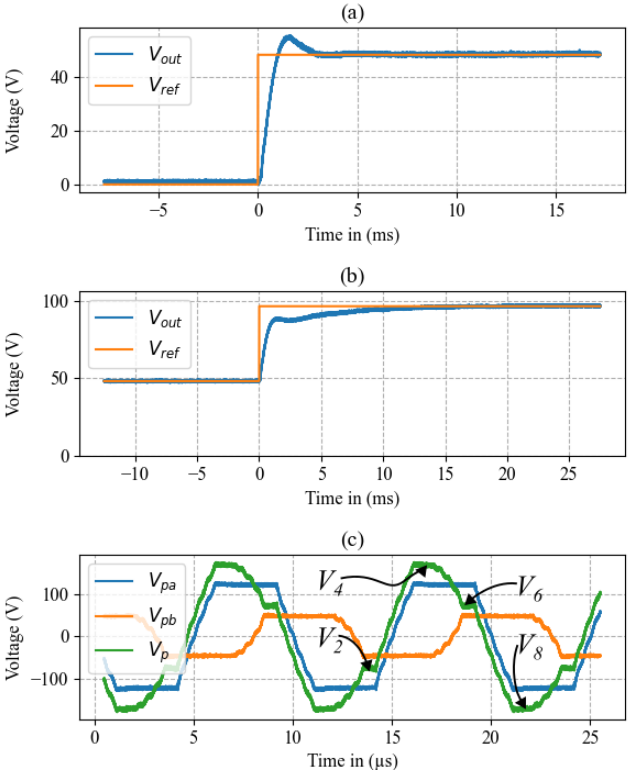

Figure 8: (a) Start operation with Vin = 120V, Vout = 48V and a 1kΩ load; (b) Fast change on Vref from 48V to 96V with Vin = 120V and a 320Ω load. (c) Converter steady state waveforms with Vin = 120V, Vout = 48V and Pout = 7W.

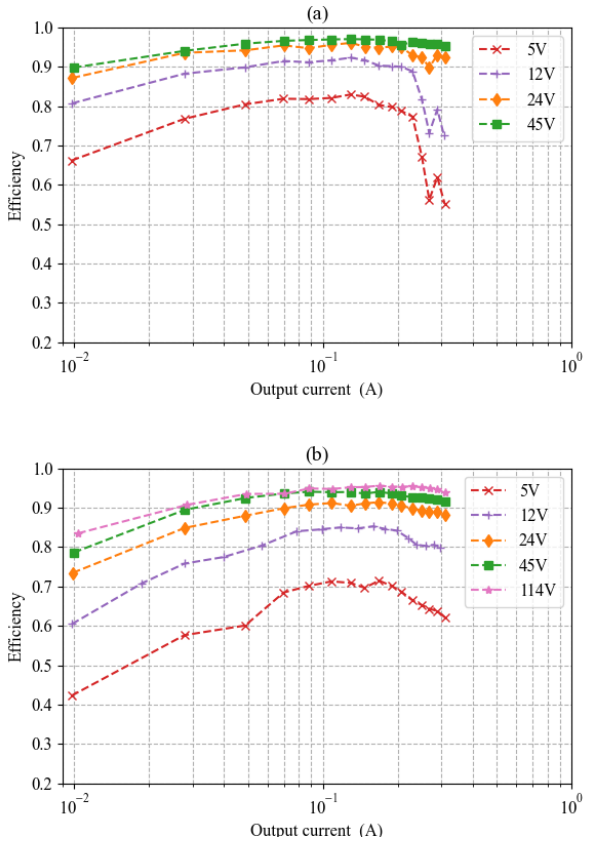

Figure 9: (a) Converter Efficiency with Vin = 48 V; (b) Converter efficiency with Vin =120V

3.2. Efficiency analyse

In this section, we measure the efficiency of the power converter only for two sets of input voltages {*48V; 120V*} for multiple output voltages {*5V; 12V; 24V; 48V; 0.95*V_{in}*}. The measurements were made using HMC8015 power analysers, and the efficiency curves are shown in Figure 9. Since piezoelectric resonators are current limited [2], we measured the efficiency in a range of output current from 10mA to 300mA without cooling system. From experiments, we analyse that in most cases the driving shift of 0.2rad were sufficient. In fact, only the conversion from 120V to 114V with output current exceeding 100mA needed an increase of the angular shifts to 0.4rad to enable ZVS and zero additional reactive power. Moreover, in comparison to the six-phase cycle proposed in [7], the new eight-phase cycle efficiency is closed. It has been observed that higher efficiency is achieved when the conversion ratio is close to one. For example, an efficiency of 95% was achieved for a 120V to 114V conversion at 30W output power. Still, for a wide range of operating points, efficiencies above 80% are achieved.

To conclude, the eight-phase converting cycle does not induce a decrease in term of power or efficiency compare to the six-phase cycle of [7], which was expected from the theoretical analysis.

Conclusion

This paper presents a new eight-phase conversion cycle applied to the DB-IPRC topology. The cycle's efficiency is demonstrated to be equal to the previously one when using a six-phase cycle. The new cycle induces the same voltage swing and the same inner useful current for a specific operating point. The eight-phase cycle also provides resilience against angles estimation errors thanks to the possibility to conduct through switches reverse diodes. Using this unique feature, we developed a new regulation loop that relies on low-frequency voltage measurements (the input and the output voltages) and a lightweight mathematical model. In the end, the converter is piloted by a single closed loop that regulates the converter output voltage. Finally, experimental measurements validate the converter's ability to converge on a steady optimal cycle.

4. References

[1] J. D. Boles, J. E. Bonavia, P. L. Acosta, Y. Ramadass, J. Lang, et D. J. Perreault, « Evaluating Piezoelectric Materials and Vibration Modes for Power Conversion », *IEEE Transactions on Power Electronics*, p. 1-1, 2021, doi: 10.1109/TPEL.2021.3114350.

[2] M. Touhami *et al.*, « Piezoelectric Materials for the DC-DC Converters Based on Piezoelectric Resonators », in *2021 IEEE 22nd Workshop on Control and Modelling of Power Electronics (COMPEL)*, nov. 2021, p. 1-8. doi: 10.1109/COMPEL52922.2021.9645999.

[3] K. Van Dyke, « The Piezo-Electric Resonator and Its Equivalent Network ». Consulté le: 17 janvier 2022. [En ligne]. Disponible sur: https://xplqa30.ieee.org/document/1670053/

[4] B. Pollet, F. Costa, et G. Despesse, « A new inductorless DC-DC piezoelectric flyback converter », in *2018 IEEE International Conference on Industrial Technology (ICIT)*, févr. 2018, p. 585-590. doi: 10.1109/ICIT.2018.8352243.

[5] M. Touhami, G. Despesse, et F. Costa, « A New Topology of DC–DC Converter Based on Piezoelectric Resonator », *IEEE Transactions on Power Electronics*, vol. 37, nº 6, p. 6986-7000, juin 2022, doi: 10.1109/TPEL.2022.3142997.

[6] J. D. Boles, J. J. Piel, et D. J. Perreault, « Enumeration and Analysis of DC–DC Converter Implementations Based on Piezoelectric Resonators », *IEEE Transactions on Power Electronics*, vol. 36, nº 1, p. 129-145, janv. 2021, doi: 10.1109/TPEL.2020.3004147.

[7] V. Breton, E. Bigot, G. Despesse, et F. Costa, « A New Isolated Topology of DC–DC Converter Based on Piezoelectric Resonators », *IEEE Transactions on Power Electronics*, vol. 38, nº 8, p. 10012-10025, août 2023, doi: 10.1109/TPEL.2023.3276478.

[8] M. Touhami, G. Despesse, F. Costa, et B. Pollet, « Implementation of Control Strategy for Step-down DC-DC Converter Based on Piezoelectric Resonator », in *2020 22nd European Conference on Power Electronics and Applications (EPE'20 ECCE Europe)*, sept. 2020, p. 1-9. doi: 10.23919/EPE20ECCEEurope43536.2020.9215910.

[9] Z. Yang, J. Forrester, J. N. Davidson, M. P. Foster, et D. A. Stone, « Resonant Current Estimation and Phase-Locked Loop Feedback Design for Piezoelectric Transformer-Based Power Supplies », *IEEE Transactions on Power Electronics*, vol. 35, nº 10, p. 10466-10476, oct. 2020, doi: 10.1109/TPEL.2020.2976206.

[10] E. A. Stolt, W. D. Braun, et J. M. Rivas-Davila, « Forward-Zero Cycle Closed-Loop Control of Piezoelectric Resonator DC-DC Converters », in *2022 IEEE 23rd Workshop on Control and Modeling for Power Electronics (COMPEL)*, juin 2022, p. 1-6. doi: 10.1109/COMPEL53829.2022.9829965.

[11] L. De Araujo Pereira, A. Morel, M. Touhami, T. Lamorelle, G. Despesse, et G. Pillonnet, « Operating Frequency Prediction of Piezoelectric DC-DC converters », *IEEE Transactions on Power Electronics*, 2021, doi: 10.1109/TPEL.2021.3115182.

[12] J. Forrester, J. N. Davidson, et M. P. Foster, « Inductorless Step-Up Piezoelectric Resonator (SUPR) Converter: A Describing Function Analysis », *IEEE Transactions on Power Electronics*, vol. 38, nº 10, p. 12874-12885, oct. 2023, doi: 10.1109/TPEL.2023.3294802.